ISSN 1674-1056
http://cpb.iphy.ac.cn
http://iopscience.iop.org/cpb
中国物理 B
Chinese Physics
中国物理 Chinese Physics B

Terahertz two-pixel imaging based on complementary compressive sensing

Yuye Wang(王与烨), Yuchen Ren(任宇琛), Linyu Chen(陈霖宇), Ci Song(宋词), Changzhao Li(李长昭), Chao Zhang(张超), Degang Xu(徐德刚), Jianquan Yao(姚建铨)

Citation: Chin. Phys. B . 2018, 27(11): 114204. **doi:** 10.1088/1674-1056/27/114204
Journal homepage: http://cpb.iphy.ac.cn; http://iopscience.iop.org/cpb

What follows is a list of articles you may be interested in

Multiple-image encryption by two-step phase-shifting interferometry and spatial multiplexing of smooth compressed signal

Xue Zhang(张学), Xiangfeng Meng(孟祥锋), Yurong Wang(王玉荣), Xiulun Yang(杨修伦), Yongkai Yin(殷永凯)
Chin. Phys. B . 2018, 27(7): 074205. **doi:** 10.1088/1674-1056/27/7/074205

Sub-Rayleigh imaging via undersampling scanning based on sparsity constraints

Chang-Bin Xue(薛长斌), Xu-Ri Yao(姚旭日), Long-Zhen Li(李龙珍), Xue-Feng Liu(刘雪峰), Wen-Kai Yu(俞文凯), Xiao-Yong Guo(郭晓勇), Guang-Jie Zhai(翟光杰), Qing Zhao(赵清)
Chin. Phys. B . 2017, 26(2): 024203. **doi:** 10.1088/1674-1056/26/2/024203

Image encryption using random sequence generated from generalized information domain

Xia-Yan Zhang(张夏衍), Guo-Ji Zhang(张国基), Xuan Li(李璇), Ya-Zhou Ren(任亚洲), Jie-Hua Wu(伍杰华)
Chin. Phys. B . 2016, 25(5): 054201. **doi:** 10.1088/1674-1056/25/5/054201

Lensless ghost imaging through the strongly scattering medium

Zhe Yang(杨哲), Lianjie Zhao(赵连洁), Xueliang Zhao(赵学亮), Wei Qin(秦伟), Junlin Li(李俊林)
Chin. Phys. B . 2016, 25(2): 024202. **doi:** 10.1088/1674-1056/25/2/024202

An iterative virtual projection method to improve the reconstruction performance for ill-posed emission tomographic problems

Liu Hua-Wei, Zheng Shu, Zhou Huai-Chun
Chin. Phys. B . 2015, 24(10): 104204. **doi:** 10.1088/1674-1056/24/10/104204

Terahertz two-pixel imaging based on complementary compressive sensing*

Yuye Wang(王与烨)[1,2,3], Yuchen Ren(任宇琛)[1,2], Linyu Chen(陈霖宇)[1,2], Ci Song(宋词)[4], Changzhao Li(李长昭)[1,2], Chao Zhang(张超)[1,2], Degang Xu(徐德刚)[1,2,†], and Jianquan Yao(姚建铨)[1,2]

[1] *Institute of Laser and Optoelectronics, School of Precision Instrument and Optoelectronics Engineering, Tianjin University, Tianjin* 300072, *China*

[2] *Key Laboratory of Optoelectronic Information Science and Technology (Ministry of Education), Tianjin University, Tianjin* 300072, *China*

[3] *Department of Neurosurgery and Key Laboratory of Neurotrauma, Southwest Hospital, Third Military Medical University (Army Medical University), Chongqing* 400038, *China*

[4] *College of Computer and Information Engineering, Tianjin Agricultural University, Tianjin* 300384, *China*

(Received 1 June 2018; revised manuscript received 12 July 2018; published online 19 October 2018)

A compact terahertz (THz) imaging system based on complementary compressive sensing has been proposed using two single-pixel detectors. By using a mechanical spatial light modulator, sampling in the transmission and reflection orientations was achieved simultaneously, which allows imaging with negative mask values. The improvement of THz image quality and anti-noise performance has been verified experimentally compared with the traditional reconstructed image, and is in good agreement with the numerical simulation. The demonstrated imaging system, with the advantages of high imaging quality and strong anti-noise property, opens up possibilities for new applications in the THz region.

Keywords: terahertz imaging, image reconstruction techniques, spatial light modulators

PACS: 42.30.Wb, 42.30.Va, 42.79.Hp **DOI:** 10.1088/1674-1056/27/11/114204

1. Introduction

The terahertz (THz) wave, between the infrared wave and the microwave wave, refers to electromagnetic radiation in the frequency range of 0.1–10 THz. Some unique characteristics have been studied and utilized in this frequency range. With the characteristic of high penetration to nonpolar material, it can be used as a light source for non-contact imaging in security inspection, anti-terrorism, and other related fields.[1] Due to the characteristic of low photon energy, THz waves are less damaging to organisms compared with x-rays, which have attracted much attention in biomedicine.

Imaging techniques plays an important role in THz wave application. Currently, point-by-point scanning imaging[2] and array imaging have been used as two kinds of mature imaging methods. The former method usually utilizes a single-pixel detector to receive the scanning signal pixel by pixel. It has the advantages of high image quality, high sensitivity, and easy accessibility. However, this kind of imaging method has an acquisition speed limitation due to Shannon's sampling theorem. It cannot meet the requirement for fast imaging. The latter method usually uses different kinds of array detectors. Although the accuracy and real-time performance of array detectors have been reported before,[3] their sensitivities cannot stand comparison with the single-pixel detector in the THz range, and the high-density detector arrays at longer wavelengths are very expensive and not easy to fabricate due to the diffraction limitation.

In recent years, single-pixel imaging schemes have been implemented based on compressive sensing (CS). As a new imaging modality, CS can easily break the limitation of Shannon's sampling theorem. The image can be reconstructed accurately with a low sampling rate. With the progress of reconstruction algorithms and the fabrication of masks, the application of CS imaging has extended from visible light and microwave to the THz region. Different THz-wave modulators such as copper-clad printed circuit boards,[4] metamaterials,[5] semiconductors,[6] and graphene[7,8] have been adopted. Due to its highly undersampled measurements, CS imaging can remedy the defect of prior imaging art in the THz range.

In the traditional THz CS imaging system, the element values of modulation matrices are always set as 0 or 1, where the physical masks may either block the THz wave or pass it to the detector. However, binary matrices with negative value would be beneficial to reduce the noise and improve the image quality.[9] Because only non-negative matrices are physically displayed by the modulators, the negative value is usually obtained through phase-sensitivity measurement utilizing a lock-in detection scheme.[10] But undesirable properties, including high cost and complicated fabrication processes, have restricted large-scale practical applications. An alternative ap-

*Project supported by the National Basic Research Program of China (Grant Nos. 2015CB755403 and 2014CB339802), the National Key Research and Development Program of China (Grant No. 2016YFC0101001), the National Natural Science Foundation of China (Grant Nos. 61775160, 61771332, and 61471257), China Postdoctoral Science Foundation (Grant No. 2016M602954), Postdoctoral Science Foundation of Chongqing, China (Grant No. Xm2016021), and the Joint Incubation Project of Southwest Hospital, China (Grant Nos. SWH2016LHJC04 and SWH2016LHJC01).

†Corresponding author. E-mail: xudegang@tju.edu.cn

© 2018 Chinese Physical Society and IOP Publishing Ltd

proach to achieve the $[1, -1]$ binary matrix is to display the $[1, 0]$ pattern followed immediately by its inverse. The difference between the two measurements is utilized to provide a differential signal,[11] which doubles the number of sampling and reduces the image speed. Recently, complementary CS imaging was employed in the visible light range by recording the data in two reflection orientations with a digital micromirror device (DMD); random $[1, -1]$ binary patterns were generated and a high-quality image was obtained. Considering the very small size of a DMD, it is not suitable for THz frequencies.

In this paper, we present a compact THz imaging system based on complementary CS. A metal mask with all modulation matrices engraved on was adopted as the spatial light modulator. The sampling in the transmission and reflection orientations was performed simultaneously using two single-pixel detectors. The $[1, -1]$ mask values were realized based on a new observed vector from the difference of the two arms data. It is shown that the THz image quality and anti-noise performance have been improved effectively. This method thus offers a very effective approach to promote the implementation of single-pixel cameras in THz applications.

2. Theory of complementary CS

CS is concerned with encoding a sparse signal using a relatively small number of linear measurements and ensures accurate reconstruction with a very high probability. The process of CS imaging can be described as an equation $\boldsymbol{y} = \boldsymbol{\Phi x} + \boldsymbol{e}$, where $\boldsymbol{x}$ represents the original signal and $\boldsymbol{e}$ is a $M \times 1$ vector of error term from random noise. When the original signal is a $N \times N$ matrix, $\boldsymbol{x}$ can be ordered as a $N^2 \times 1$ vector. $\boldsymbol{\Phi}$ represents a $M \times N^2$ measurement matrix, and $\boldsymbol{y}$ is a $M\times$ 1 vector formed by M time measurements. M is calculated by $O\left(K \cdot \log\left(N^2/K\right)\right)$. $\boldsymbol{x}$ is K-order sparse, where $K < M \ll N^2$. In order to ensure the signal is reconstructed from M observed values, the restricted isometry property[12] is a prerequisite when the measurement matrix satisfies certain conditions. Then, the recovery of the sparse signals can be realized using different algorithms, such as total variation regularization, orthogonal matching pursuit,[13] basis pursuit,[14] and l_p-norm.[15]

Generally, because only non-negative matrices can be displayed by a physical mask, $\boldsymbol{\Phi}$ is always structured with the value 0 or 1 for each pixel, corresponding to opaque and transparent mask regions, respectively. Thus, part of the light flux is sacrificed and the noise is increased. In order to improve the image quality and the signal-to-noise ratio (SNR), a complementary measurement method is given to use two complementary sets of masks.[16] It can be described as

$$\boldsymbol{y}_1 = \boldsymbol{\Phi}_1 \boldsymbol{x} + \boldsymbol{e}_1, \tag{1}$$

$$\boldsymbol{y}_2 = \boldsymbol{\Phi}_2 \boldsymbol{x} + \boldsymbol{e}_2, \tag{2}$$

where $\boldsymbol{\Phi}_1 = \mathbf{1}_{M\times N^2} - \boldsymbol{\Phi}_2$ ($\mathbf{1}_{M\times N^2}$ denotes an array of all ones), and $\boldsymbol{e}_1$ together with $\boldsymbol{e}_2$ corresponds to the noise in the different directions respectively. Taking the subtraction between equations (1) and (2), we can have the following formula:

$$\boldsymbol{y}_1 - \boldsymbol{y}_2 = (\boldsymbol{\Phi}_1 - \boldsymbol{\Phi}_2)\boldsymbol{x} + (\boldsymbol{e}_1 - \boldsymbol{e}_2). \tag{3}$$

Since $\boldsymbol{\Phi}_1$ and $\boldsymbol{\Phi}_2$ are complementary matrices with values 1 and 0, $\boldsymbol{\Phi}_1 - \boldsymbol{\Phi}_2$ can be seen as a $[1, -1]$ matrix. Thus, the elements of measurement matrix $\boldsymbol{\Phi} = \boldsymbol{\Phi}_1 - \boldsymbol{\Phi}_2$ are all nonzero, and the THz throughput and modulation efficiency are optimized. Meanwhile, because most of the noises in $\boldsymbol{e}_1$ and $\boldsymbol{e}_2$ caused by the power fluctuation of THz source, the complex environments, and so on, are correlated with each other during the measurement of the $M \times 1$ vector, the random noise level is reduced as $\boldsymbol{e} = \boldsymbol{e}_1 - \boldsymbol{e}_2$. Considering the uncorrelated noises caused by the detectors take a small proportion in $\boldsymbol{e}_1$ and $\boldsymbol{e}_2$ compared with the THz power fluctuation, they can be reduced by taking several THz pulses for the average in each measurement. Therefore the synchronous measurements for the two sets with two detectors are preferred for minimizing the impact of noise. The advantage of this method is that it can be applied equally when the measurement matrix $\boldsymbol{\Phi}$ is designed as $[\sigma, -\sigma]$.

3. Numerical simulations

For verifying the validity of the complementary CS imaging method, the reconstructions of 'H' and 'O' were simulated as shown in figure 1(a). The resolution was 20×20 pixels for each letter. The TVAL3 algorithm[17] was chosen for reconstruction. The calculation parameters were set the same as those used in the following recovery of THz CS imaging in section 5. The measurement matrix consisting of two values 0 or 1 was structured based on the Gaussian matrix which has little coherence with the Walsh–Hadamard matrix. Figures 1(b) and 1(c) show the images reconstructed by the conventional single CS using 20% data measurements with $[1, 0]$ and $[0, 1]$ sets, respectively. Figure 1(d) is the reconstructed image employing complementary CS imaging with $[1, -1]$ set. Based on visibility by human judgment, the reconstructed images in figure 1(d) are almost the same as the original images in figure 1(a), and better than those in figures 1(b) and 1(c). To evaluate the reconstructed image quality more objectively, the peak signal to noise ratio (PSNR) was computed. Commonly, the larger the PSNR value, the better the quality of the recovered image. It is clear that the PSNRs of the recovered images for H and O under single CS mode are not very different from each other. However, the PSNR of figure 1(d) is much larger than that of figures 1(b) and 1(c), and more than three times larger for O. Therefore, the complementary CS imaging has the advantage of better image quality.

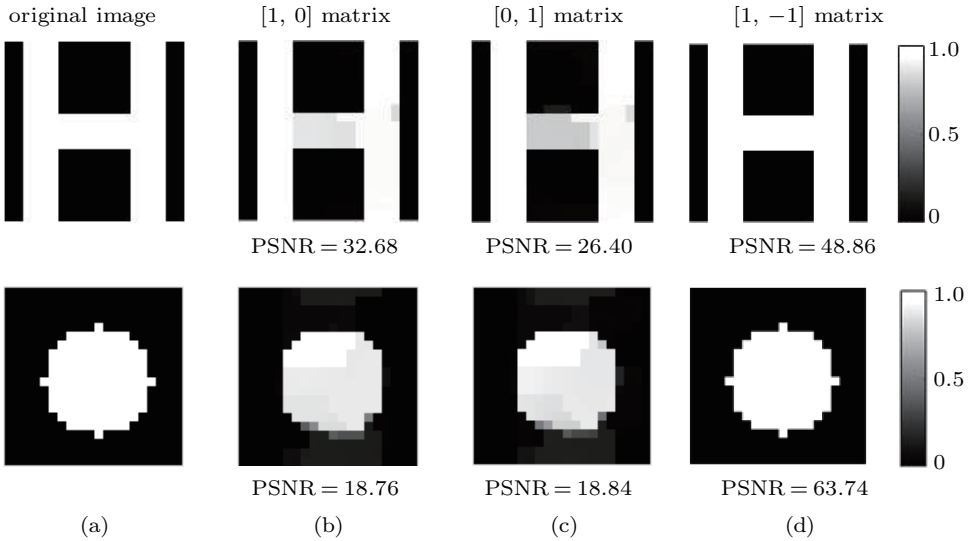


Fig. 1. Simulation results of CS reconstruction using measurement matrix with different values: (a) original image, (b) $[1, 0]$ matrix, (c) $[0, 1]$ matrix, (d) $[1, -1]$ matrix.

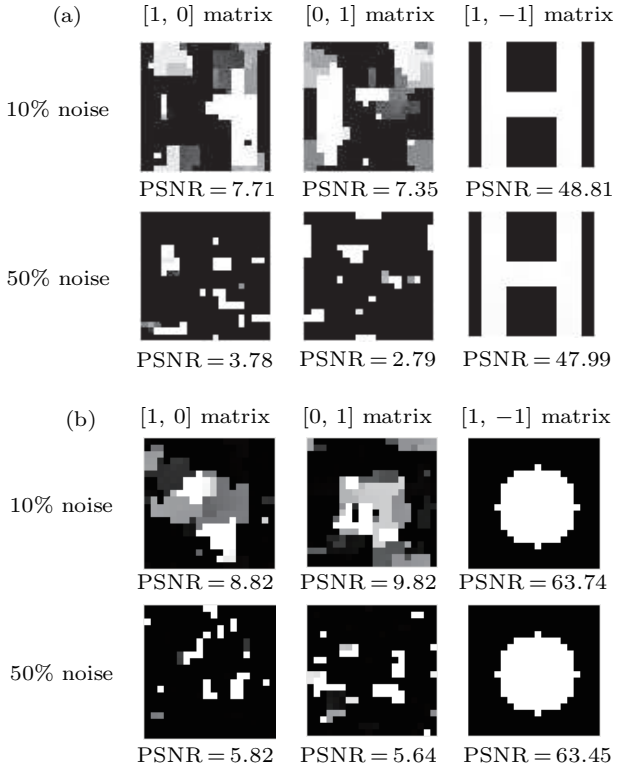


Fig. 2. Simulation results of CS reconstruction for (a) H and (b) O with 10% and 50% Gaussian noises added.

Moreover, to analyze the anti-noise performance, 10% and 50% Gaussian noise was superimposed upon the measurement vectors $\boldsymbol{y}$ respectively for H and O. The results based on the three methods are shown in figure 2. The integrity and PSNR of the reconstructed images were distinctly degraded with the noise level increase. Comparatively speaking, the deterioration degree of the reconstructed images was much more serious for the conventional single CS with both the $[1, 0]$ and $[0, 1]$ set. The recovered letters were unrecognizable under the situation of 10% Gaussian noise, and even worse under the situation of 50% Gaussian noise. However, by the method of complementary CS imaging, the reconstructed letters can both be easily recognized with 10% and 50% Gaussian noise; the quality of the recovered image decreased a little for H and was almost unchanged for O. This can be attributed to the subtraction of the two measured vectors. In this sense, the anti-noise performance of complementary CS imaging is much better than that of conventional single CS imaging.

4. Experimental setup

The design of the complementary CS imaging system is presented in figure 3(a). The THz radiation was generated by a continuous wave THz gas laser. The output frequency of the THz radiation was fixed at 2.52 THz and the output power was about 40 mW in our experiment. The THz wave was chopped into 50 Hz by a chopper, passed through the object, and imaged onto the mask at the angle of 45° with respect to the normal incidence. The mask was a piece of stainless steel with a 20×99 Gaussian random matrix made of 0 and 1 engraved on, the same as that in [18]. It can split the THz wave into a transmission path and a reflection path. The size of the mask was 150 mm long, 30 mm wide, and 0.1 mm thick. In order to avoid the diffraction effect at the mask, the 0.45 mm×0.45 mm square hollow matched to value 1 in the matrix, and those without processing corresponded to value 0. Each column of the matrix was uncorrelated, which can guarantee the original signal was reconstructed well because of the low relativity of the Walsh–Hadamard transform matrix and Gaussian random measurement matrix. The encoding process was achieved by physically translating the mask with a one-dimensional linear motor stage. The measurement matrices for the two paths were complementary.

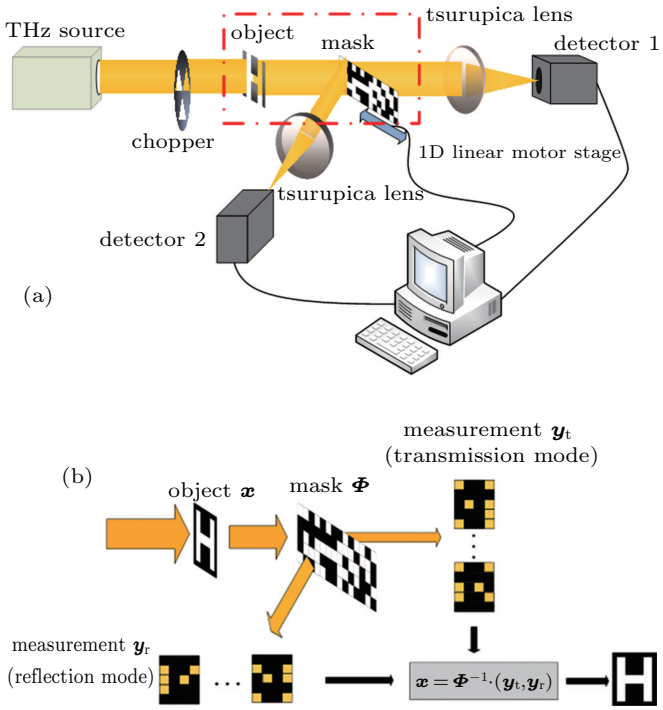


Fig. 3. (color online) (a) Experimental apparatus for complementary compressive imaging using a metal mask and two Golay cell detectors; (b) Details of generating the $[1, -1]$ matrix using a metal mask.

A total of 80 different matrices with a size of 20×20 can be obtained by just horizontally moving the mask by one column each time. The transmitted and reflected THz waves through the mask were further focused using a Tsurupica lens and sensed by Golay cell detectors synchronously. Figure 3(b) is the detailed schematic diagram for the dotted area in figure 3(a); one detector responded to the energy transmitted by the mask, whereas the other received the energy reflected from the same mask. The string of values, collected by measuring the transmission intensity (y_{ti}) and reflection intensity (y_{ri}) for each mask, represents the image encoded within the mask's features, where $i = 1, 2, \ldots, 80$. The desired encoding $\boldsymbol{y}$, containing 80 elements y_1, y_2,...,y_{80}, can be obtained by the difference between the two measurement vectors $\boldsymbol{y}_r$ and $\boldsymbol{y}_t$. The image can be retrieved from the encoded data by a reconstruction algorithm based on $\boldsymbol{x} = \boldsymbol{\Phi}^{-1}\boldsymbol{y}$. Such a system has the advantages of overall doubling of THz throughput efficiency because no flux is wasted by opaque mask pixels.

5. Results and discussion

Considering that the beam quality plays an important role in CS imaging, the intensity distribution of the THz wave was measured. A metal sheet with a 1 mm diameter pinhole was fixed on a two-dimensional linearmotor stage to scan the THz beam. The energy distribution is shown in figure 4. The horizontal and vertical cuts through the center of the beam, shown on the map as black dotted lines, are displayed. The full width at half-maximum beam diameters of 4 mm and 10 mm were observed in the horizontal and vertical directions, respectively. Due to the intensity necessary in the complementary CS imaging system, no beam expander was set to keep the high SNR for the detections in the two radiation paths. Thus, the samples with proper sizes were placed in the energy concentration area. If a sample with large number of pixels was imaged, the beam expander was inserted to make the THz beam illuminate the whole object homogeneously.But this will result in a lower energy density, which directly leads to a lower SNR.

In order to investigate the influence of noise on the reconstructed images, the energy fluctuation of the THz source was measured. It is one of the main noise-induced factors for the imaging system. Figure 5 shows the stability of the THz output with 1, 5, 10, 15, and 20 pulses on average. The standard deviations were 0.0358, 0.0171, 0.0120, 0.0099, and 0.0087, respectively. It is clear that the standard deviation decreased rapidly from 1 pulse to 10 pulses, but slowly from 10 pulses to 20 pulses. Considering the reduction of the acquisition time without sacrificing the reconstruction quality, 10 pulses were taken as the average in our experiment.

Figure 6 shows the process that generates the complementary CS images. To make the asymmetric THz beam illuminate the whole object as uniformly as possible, parts of the hole-shaped letter H with size 4 mm× 6 mm and a hole

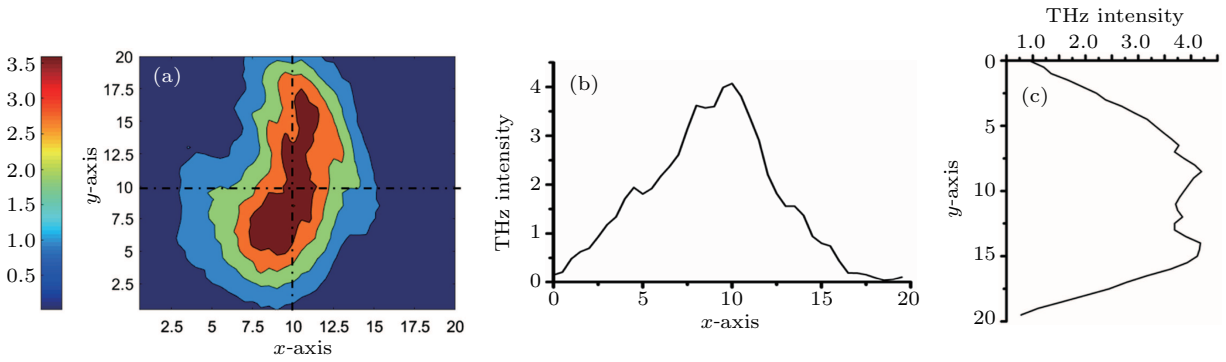


Fig. 4. (color online) (a) Energy distribution of THz radiation source, (b) and (c) the horizontal and vertical cuts through the center of the beam.

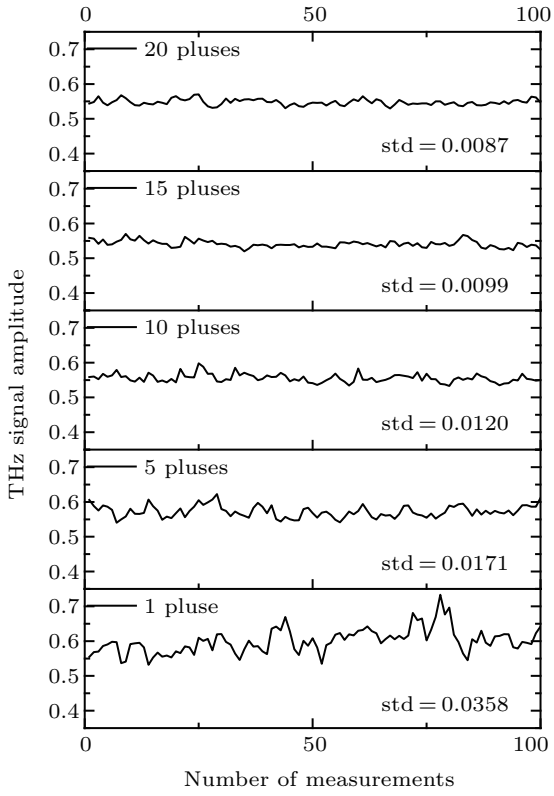


Fig. 5. Instability of the THz source.

with a diameter of 4 mm were tested. Figure 6(a) shows the visual images of the objects, where the imaged parts are indicated by the red lines and the other parts are covered by the multilayer aluminum foil to block the THz wave. Figures 6(b) and 6(c) illustrate the images recovered from the data in transmission and reflection orientations. The complementary CS images are shown in figure 6(d). By comparing figure 6(d) with figures 6(b) and 6(c), it is clear that the complementary CS image gives better visibility. The PSNR of the recovered images in figures 6(b) and 6(c) under single CS detection do not differ greatly from each other, whereas the PSNR of figure 6(d) is much larger than that of figures 6(b) and 6(c). The result is in good agreement with the numerical simulation. The size of the recovered images can be obtained by counting the pixels since each pixel corresponds to a 0.5 mm area. For the transverse rectangle in the first row of figure 6(a), the sizes of the reconstructed images from the transmission and reflection directions were both 2.5 mm×3.5 mm, which is a little shorter than the original image of 2 mm×4 mm, while the recovery using complementary CS image yielded an image of 2.5 mm×4 mm, much closer to the original image. For the vertical rectangle in the second row of figure 6(a), the reconstruction quality was significantly improved according to the value of the PSNR and the rectangle edges were finely preserved based on the complementary CS image. Moreover, the corner-shaped structure in the third row of figure 6(a) was tested. The original shape cannot be well recognized from any single orientation. Although there were some defects on the right edge of the reconstructed structure by complementary CS imaging, it still performed much better than the conventional method. It is noted that a 4 mm diameter hole pattern in the fourth row of figure 6(a) can be recognized based on these three sets of data intuitively. But the image recovered by complementary CS imaging consisted of smoother regions with much sharper edges, and the recovered size was equal to that of the actual image, whereas there was still some deviation for the single arm detection. Thus, it is evident that complementary CS imaging can improve the image quality dramatically compared with the traditional reconstructed image.

To prove the anti-noise performance of complementary CS imaging, different numbers of the averaged pulses were used for the reconstruction of the vertical rectangle in figure 6(a) under identical detection conditions. Figure 7 shows the experimental reconstructed results by single CS in transmission and reflection directions, and the complementary CS image at a 20% sampling rate with 1, 5, 10, 15, and 20 pulses on average for one measurement, respectively. The image quality of these methods all increased with the increase of the average pulse number from 1 to 10. Meanwhile, almost no better quality was obtained by further increasing the average pulse number from 10 to 20. Noise decreasing and tendency to be stable with the increase of the average pulse number were deduced to be the reasons. Therefore, we can discern that ten pulses or more for each sampling will bring a relatively stable recovered image quality. Furthermore, under the same average pulse number, the image quality of the complementary CS image in figure 7(c) was always better than that recovered from the two orientations in figure 7(a) and 7(b). In this sense, the complementary CS imaging method has stronger anti-noise property. In addition, it is evident that the total number of measurements needed in complementary CS imaging is much smaller than that in single-pixel sampling methods in order to obtain the same PSNR value.

The images reconstructed in our experiment are not as perfect as the simulation results. We deduce that this is mainly caused by the inhomogeneous distribution of THz beam energy and the THz energy loss by the mask. On one hand, most of the reconstruction algorithms can be well applied in the assumption that the light is a plane wave, which is hardly satisfied in the THz experiments. On the other hand, the mask was fabricated by engraving the matrix on a piece of metal sheet using etching technology. Polishing and high reflection coating in THz range cannot be easily performed due to the small size of each pixel unit (0.45 mm×0.45 mm). Actually, diffuse reflections are generated when the THz beam illuminates the rough surface of the mask. Thus, the sum of the detected energies from two directions is not a constant. In other words, the noise is introduced and it will cause the loss of image quality.

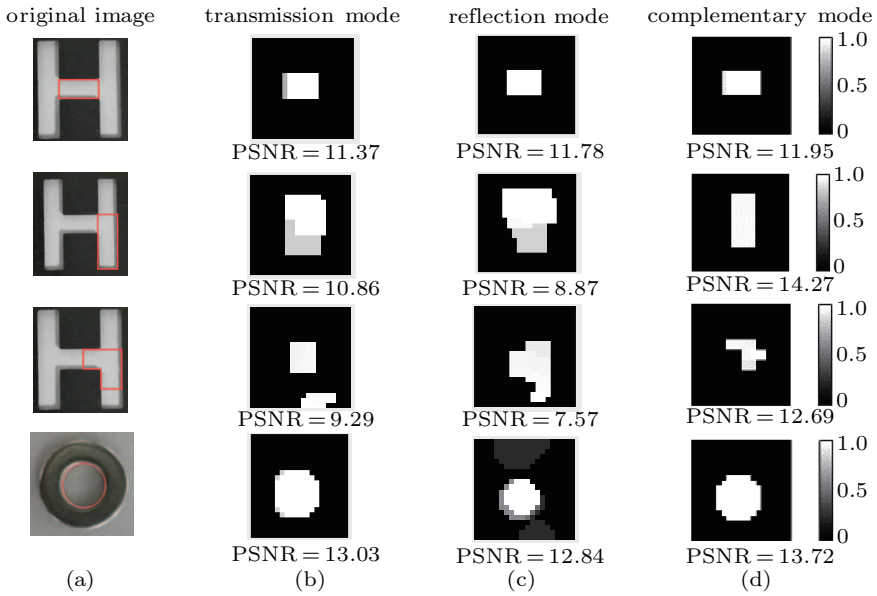


Fig. 6. (color online) Reconstruction results of four different objects: (a) original image, (b) transmission mode, (c) reflection mode, (d) complementary mode.

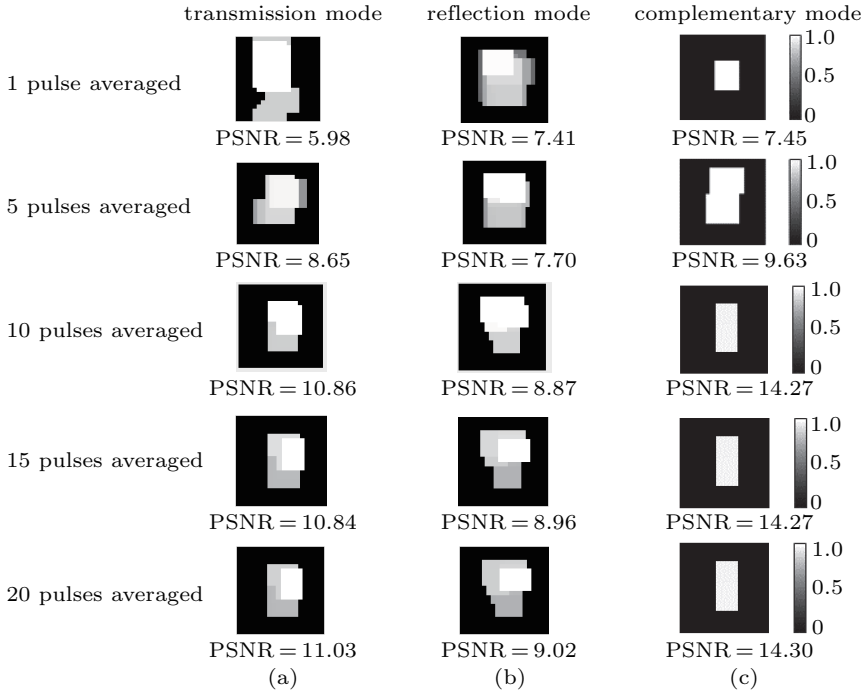


Fig. 7. The experimental reconstructed results by different numbers of pulses averaged: (a) transmission mode, (b) reflection mode, (c) complementary mode.

6. Conclusion

We have demonstrated a compact THz imaging system based on complementary CS sensing. Compared with the conventional single-pixel camera with one detection orientation, our scheme makes full use of the encoded THz energy through both transmission and reflection directions. The image can be reconstructed based on a new observed vector from the difference of the two arms data, which permits imaging with negative mask values. We have experimentally investigated the THz image quality and anti-noise performance of complementary CS imaging. It is evident that THz two-pixel imaging with complementary compressive sensing has the advantages of higher imaging quality and THz throughput efficiency, along with stronger anti-noise property. It is expected to promote the implementation of single-pixel cameras in THz applications.

References

[1] Luukanen A, Leivo M, Tamminen A, Dietlein C R and Grossman E N 2010 *Proceedings of SPIE the International Society for Optical Engineering*, April 8, 2010, Orlando, America, p. 7670
[2] Hu B B and Nuss M C 1995 *Opt. Lett.* **20** 1716
[3] Friederich F, Spiegel W, Bauer M, Meng F, Thomson M D, Boppel S, Lisauskas A, Hils B, Krozer V, Keil A, Loffler T, Henneberger R, Huhn

A K, Spickermann G, Bolivar P H and Roskos H G 2014 *IEEE Trans. Terahertz Sci. Technol.* **1** 183

[4] Chan W L, Charan K, Takhar D, Kelly K F, Baraniuk R G and Mittleman D M 2008 *Appl. Phys. Lett.* **93** S293

[5] Nadell C C, Watts C M, Montoya J A, Krishna S and Padilla W J 2016 *Adv. Opt. Mater.* **4** 66

[6] Phillips D B, Hendry E, Padgett M J, Hobson P, Stantchev R I and Hornett S M 2017 *Optica* **4** 989

[7] Sensale-Rodriguez B, Rafique S, Yan R S, Zhu M D, Protasenko V, Jena D, Liu L and Xing H G 2013 *Opt. Express* **21** 2324

[8] Yan X, Liang L J, Zhang Z, Yang M S, Wei D Q, Wang M, Li Y P, Lü Y Y, Zhang X F, Ding X and Yao J Q 2018 *Acta Phys. Sin.* **67** 118102 (in Chinese)

[9] Harwit M 1979 *Hadamard Transform Optics* (Cambridge: Academic Press) pp. 96–108

[10] Watts C M, Shrekenhamer D, Montoya J, Lipworth G, Hunt J, Sleasman T, Krishna S, Smith D R and Padilla W J 2014 *Nat. Photon.* **8** 605

[11] Davis D S 1995 *Appl. Opt.* **34** 1170

[12] Candes E J 2008 *C. R. Math.* **346** 589

[13] Tropp J A and Gilbert A C 2007 *IEEE Trans. Inf. Theory* **53** 4655

[14] Donoho D L 2006 *IEEE Trans. Inf. Theory* **52** 1289

[15] Ning F L, He B J and Wei J 2013 *Acta Phys. Sin.* **62** 174212 (in Chinese)

[16] Yu W K, Liu X F, Yao X R, Wang C, Zhai Y and Zhai G J 2015 *Sci. Rep.* **4** 5834

[17] Li C 2009 *An efficient algorithm for total variation regularization with applications to the single pixel camera and compressive sensing* (MS Dissertation) (Houston: Rice University)

[18] Duan P, Wang Y Y, Xu D G, Yan C, Yang Z, Xu W T, Shi W and Yao J Q 2016 *Appl. Opt.* **55** 3670